(Preprint) AAS 21-511

SATELLITE RELATIVE STATE UNCERTAINTY DYNAMICS IN THE VICINITY OF A POORLY TRACKED TARGET OBJECT

Ethan R. Burnett* **and Hanspeter Schaub†**

This paper explores the dynamics for the sensitivity of the satellite relative state to uncertainty in the initial orbit elements of the target object about which the dynamics have been linearized. These sensitivities enable rapid and highly accurate Monte Carlo analysis of the evolving uncertainty in the relative state with respect to a nearby unknown target object. The dynamics of the sensitivities are derived, and the influence of control on these quantities is investigated. Because the sensitivities directly determine the time-varying shape of the relative state distribution, the interesting concept of using control to directly influence the sensitivities is also explored. Through this framework, the uncertainty distribution of relative states can be directly influenced to some degree, which could be useful in some rendezvous and relative motion applications.

INTRODUCTION

A major topic in formation flying and satellite proximity operations is collision avoidance with other space objects. There have been many important works studying the effects of uncertainties in the satellite relative motion problem. Reference 7 derives analytic uncertainty propagation for the relative motion problem in elliptic orbits. Under the assumption of a Gaussian white noise process, they explore the computation of the evolving mean and covariance matrix of the relative states using Tschauner-Hempel equations.[10] Some work has focused on designing guidance and control to mitigate collision risks in the presence of uncertainties, both with active and passive methods. A classic passive means of minimizing impact risk in formation flying is through the safe ellipse, which ensures that in the presence of along-track drift in the relative motion, the spacecraft will not collide.[6] In Reference 1, Breger and How investigate tradeoffs between active and passive approaches to safety. They also develop a strategy for generating safe, fuel-optimized rendezvous trajectories that guarantee collision avoidance for a large class of anomalous behaviors. Reference 4 develops a Receding Horizon Control (RHC) approach that enforces passive safety in the presence of common navigation or propulsive system failures. They identify that adding cross-track relative motion also greatly reduces collision probability.

There are several works which explore the problem of rendezvous and proximity operations when the target orbit is uncertain, which leads to uncertainty in the linearized model. In these works, the spacecraft relative state is assumed to be directly and accurately measured, but the effects of dynamic uncertainty need to be mitigated. Reference 8 studies reliable impulsive state-feedback

*Research Assistant, NDSEG Fellow, Ann and H.J. Smead Department of Aerospace Engineering Sciences, University of Colorado Boulder, Boulder, CO, 80309 USA.

†Glenn L. Murphy Chair of Engineering, Smead Department of Aerospace Engineering Sciences, University of Colorado, 431 UCB, Colorado Center for Astrodynamics Research, Boulder, CO 80309-0431. AAS Fellow, AIAA Fellow.

control for autonomous spacecraft rendezvous under target orbital uncertainty with the possibility of thruster faults. This is accomplished using Lyapunov theory and genetic algorithms. Reference 11 addresses robust H_∞ control for spacecraft rendezvous with a noncooperative target, specifically for the case of CW dynamics, in which the target semimajor axis is uncertain. The control design enables rendezvous in the presence of this dynamical uncertainty, while also allowing for control input saturation. In both References 8 and 11, the uncertainty in the target orbit manifests only as dynamic uncertainty in the linearized models. The relative position and velocity are assumed to be observable.

Typically, the safe use of translational control in close proximity requires that the relative position and velocity be directly and accurately observed, otherwise there is a fundamental risk of collision or other undesired outcomes. However, sometimes a spacecraft must maneuver in the vicinity of another space object whose position and velocity is not known to a desirable degree of accuracy, due to poor observability conditions or any other factors leading to an inability to make the necessary measurements. In such circumstances, the initial estimates of the relative state are going to have some degree of error, and the resulting relative motion over time will be generally uncertain as well. This is depicted in Figure 1, where the nominal relative position $\boldsymbol{\rho}^*$ obtained from the best guess of the target orbit differs from the true relative state $\boldsymbol{\rho}$. In addition to dynamic error due to incorrect linearization, the uncertainty directly affects the relative range and range rate, as well as the orientation of the target-centered LVLH frame. This paper studies this problem of relative motion in the vicinity of a poorly tracked target object, from the perspective of the linear sensitivities of the relative state. The sensitivities studied are the derivative of the relative state vector with respect to the individual uncertain orbit elements of the target spacecraft, and they have their own linear forced dynamics if the two spacecraft are in close proximity in similar orbits.

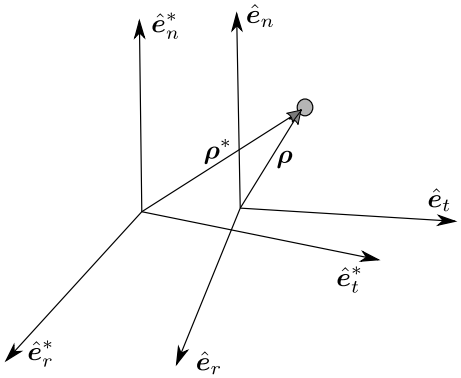

Figure 1: Relative Position from Estimated and True Target Spacecraft Locations

Through the sensitivities, an uncertainty distribution in the initial target orbit elements can be directly mapped to an evolving uncertainty distribution in the relative state. Assuming small target orbit element errors, the problem can be approached by linearization, and the sensitivities progress with their own dynamics influenced only by the nominal relative state and by the control. The action of an estimator has no effect on the sensitivity propagation, and instead changes the uncertainty distribution of the initial target orbit elements. In this manner, the sensitivities act as a scaffolding for the relative state uncertainty distribution, and only need to be propagated once in parallel with the nominal relative motion dynamics. This framework could allow for uncertainty-conscious linear control to be designed for the relative motion problem that actively reduces the risk of satellite

impact due to errors in the target orbit estimate.

SENSITIVITY DYNAMICS

Fundamentals of the Linear Sensitivities

The relative state of a satellite with respect to another orbiting space object is a function of the orbit elements of the two. Let $\mathbf{oe}_s$ and $\mathbf{oe}_t$ denote the controlled spacecraft and the target object's orbit elements at some epoch time. For linearization about an incorrect orbit parameterized by estimated target orbit elements $\mathbf{oe}_t^*$, the true relative state $\boldsymbol{x}$ can be expressed as a sum of the nominal state $\boldsymbol{x}^*$ and the deviations induced by the product of the sensitivities to the orbit elements and their errors:

$$\boldsymbol{s}_i = \left.\frac{\mathrm{d}\boldsymbol{x}}{\mathrm{d}oe_{t,i}}\right|_* \tag{1}$$

$$\check{\boldsymbol{s}}_i = \left.\frac{\mathrm{d}\boldsymbol{x}}{\mathrm{d}oe_{s,i}}\right|_* \tag{2}$$

$$\begin{aligned}\boldsymbol{x} &\approx \boldsymbol{x}^* + \left.\frac{\mathrm{d}\boldsymbol{x}}{\mathrm{d}\mathbf{oe}_t}\right|_* (\mathbf{oe}_t - \mathbf{oe}_t^*) + \left.\frac{\mathrm{d}\boldsymbol{x}}{\mathrm{d}\mathbf{oe}_s}\right|_* (\mathbf{oe}_s - \mathbf{oe}_s^*) \\ &= \boldsymbol{x}^* + \sum_{i=1}^{6} \left(oe_{t,i} - oe_{t,i}^*\right) \boldsymbol{s}_i + \sum_{i=1}^{6} \left(oe_{s,i} - oe_{s,i}^*\right) \check{\boldsymbol{s}}_i\end{aligned} \tag{3}$$

In this work, the orbit of the maneuvering spacecraft is assumed to be known to much higher precision than the target orbit, so the influence of this uncertainty on the relative state is neglected:

$$\boldsymbol{x} \approx \boldsymbol{x}^* + \sum_{i=1}^{6} \left(oe_{t,i} - oe_{t,i}^*\right) \boldsymbol{s}_i \tag{4}$$

The "t" subscript is dropped, because this work only considers uncertainties in the orbit elements of the unknown target object's orbit. The associated sensitivity state vectors have their own linear forced dynamics, obtained from the relative motion dynamics.

$$\dot{\boldsymbol{s}}_i = \frac{\mathrm{d}}{\mathrm{d}t}\left(\frac{\mathrm{d}\boldsymbol{x}}{\mathrm{d}oe_i}\right) = \frac{\mathrm{d}}{\mathrm{d}oe_i}\left(\frac{\mathrm{d}\boldsymbol{x}}{\mathrm{d}t}\right) = \frac{\mathrm{d}}{\mathrm{d}oe_i}\left(A_{\boldsymbol{x}}\right)\boldsymbol{x} + A_{\boldsymbol{x}}\boldsymbol{s}_i + \frac{\mathrm{d}}{\mathrm{d}oe_i}\left(B_{\boldsymbol{x}}\right)\boldsymbol{u} \tag{5}$$

Note that the concept of sensitivities having their own dynamics is not new, and is explored extensively in Reference 5.

Dynamics in Local Cartesian Coordinates

If the relative state $\boldsymbol{x}$ is in Cartesian coordinates in the LVLH frame, the plant matrix $A_{\boldsymbol{x}}$[9] and control matrix $B_{\boldsymbol{x}}$ are given below for the Keplerian case.

$$A_{\boldsymbol{x}} = \begin{bmatrix} 0 & 0 & 0 & 1 & 0 & 0 \\ 0 & 0 & 0 & 0 & 1 & 0 \\ 0 & 0 & 0 & 0 & 0 & 1 \\ \dot{\theta}^2 + 2\frac{\mu}{r^3} & \ddot{\theta} & 0 & 0 & 2\dot{\theta} & 0 \\ -\ddot{\theta} & \dot{\theta}^2 - \frac{\mu}{r^3} & 0 & -2\dot{\theta} & 0 & 0 \\ 0 & 0 & -\frac{\mu}{r^3} & 0 & 0 & 0 \end{bmatrix} \tag{6}$$

$$B_{\boldsymbol{x}} = \begin{bmatrix} 0_{3\times 3} \\ R_3(\theta)R_1(i)R_3(\Omega)R^*_{\mathcal{NH}} \end{bmatrix} \tag{7}$$

In Eq. (7), the rotation matrix $R^*_{\mathcal{NH}}$ maps from the known nominal LVLH frame to the inertial frame, and the subsequent rotations map from the inertial frame to the true LVLH frame. For small uncertainties in the target orbit, the lower 3×3 sub-matrix in $B_{\boldsymbol{x}}$ will thus be close to identity. The sensitivity dynamics given by Eq. (5) are evaluated using a chosen nominal target orbit and nominal relative motion, and are not influenced by the uncertainty in the target orbit elements. Note that the last term in Eq. (5) is nonzero only for the sensitivities to the orbit element angles parameterizing the rotation $R_{\mathcal{HN}}$ from the inertial frame $\mathcal{N}$ to the target-centered LVLH frame $\mathcal{H}$.

The initial values of the sensitivities will typically be nonzero for this problem, and can be directly computed. References 9 and 3 discuss the geometric method, mapping the relative state in orbit element differences to the relative state in local Cartesian or curvilinear coordinates via the linear mapping $\boldsymbol{x} = [G(\theta)]\,\delta\mathbf{oe}$. Writing $\boldsymbol{x}^*_0 = [G(\theta_0)]\,\delta\mathbf{oe}^*_0$, where $\delta\mathbf{oe}^*_0 = \mathbf{oe}_s(0) - \mathbf{oe}^*_t(0)$, the initial sensitivities are derived:

$$\boldsymbol{s}_i(0) = \frac{\mathrm{d}\boldsymbol{x}^*_0}{\mathrm{d}\,\text{œ}_i(0)} = \frac{\mathrm{d}}{\mathrm{d}\,\text{œ}_i(0)}\left(G(\theta_0)\,\delta\mathbf{oe}^*_0\right) = \frac{\mathrm{d}}{\mathrm{d}\,\text{œ}_i(0)}\left(G(\theta_0)\right)\delta\mathbf{oe}^*_0 + G(\theta_0)\frac{\mathrm{d}\,\delta\mathbf{oe}^*_0}{\mathrm{d}\,\text{œ}_i(0)} \tag{8}$$

$G(\theta)$ is reproduced below from Reference 9 for when $\boldsymbol{x}$ is in local Cartesian coordinates and $\delta\mathbf{oe}$ is in quasi-nonsingular orbit element differences:

$$G_{\boldsymbol{x}} = \begin{bmatrix} \frac{r}{a} & \frac{v_r}{v_t}r & 0 & -\frac{r}{p}(2aq_1 + r\mathrm{c}\theta) & -\frac{r}{p}(2aq_2 + r\mathrm{s}\theta) & 0 \\ 0 & r & 0 & 0 & 0 & r\mathrm{c}i \\ 0 & 0 & r\mathrm{s}\theta & 0 & 0 & -r\mathrm{c}\theta\mathrm{s}i \\ -\frac{v_r}{2a} & \left(\frac{1}{r} - \frac{1}{p}\right)h & 0 & \frac{1}{p}(v_r a q_1 + h\mathrm{s}\theta) & \frac{1}{p}(v_r a q_2 - h\mathrm{c}\theta) & 0 \\ -\frac{3v_t}{2a} & -v_r & 0 & \frac{1}{p}(3v_t a q_1 + 2h\mathrm{c}\theta) & \frac{1}{p}(3v_t a q_2 + 2h\mathrm{s}\theta) & v_r\mathrm{c}i \\ 0 & 0 & (v_t\mathrm{c}\theta + v_r\mathrm{s}\theta) & 0 & 0 & (v_t\mathrm{s}\theta - v_r\mathrm{c}\theta)\mathrm{s}i \end{bmatrix} \tag{9}$$

where $v_r = \dot{r}$, $v_t = r\dot{\theta}$, and c and s denote the cos and sin functions respectively. Because of the definition of $\delta\mathbf{oe}^*_0$, the final term in Eq. (8) can be rewritten as $-G(\theta_0)\hat{\boldsymbol{e}}_i$, where $\hat{e}_i$ is a unit vector with six components, with the i^{th} component one and all other components zero. Note from Eq. (5) that the sensitivity state vectors behave as an augmented position and velocity vector. In other words, for the elements s_j of a given sensitivity vector, $\dot{s}_j = s_{j+3}$ for $j = 1,\ 2,\ 3$.

Denoting $\Delta\,\mathbf{oe} = \mathbf{oe} - \mathbf{oe}^*$, and writing each $\boldsymbol{s}_i$ in terms of its associated element œ_i, Eq. (3) is rewritten in terms of the sensitivities to and differences in the initial target quasi-nonsingular orbit elements $\mathbf{oe}_0$:

$$\boldsymbol{x} = \boldsymbol{x}^* + \boldsymbol{s}_a\Delta a + \boldsymbol{s}_{\theta_0}\Delta\theta_0 + \boldsymbol{s}_i\Delta i + \boldsymbol{s}_{q_1}\Delta q_1 + \boldsymbol{s}_{q_2}\Delta q_2 + \boldsymbol{s}_\Omega\Delta\Omega \tag{10}$$

Because the target spacecraft orbit is parameterized by epoch orbit elements, an initial statistical distribution in these epoch elements can be directly mapped to a distribution of future relative states via the sensitivities $\boldsymbol{s}_i$.

In Eq. (10), the relative state is expressed as a time-varying vector sum of scalar random variables. This is interesting because in principle, for the unforced problem, the time-varying vector states can be computed analytically as functions of the nominal target argument of latitude θ for the case of Keplerian orbits. This would enable highly efficient uncertainty propagation for the problem of close-proximity spacecraft relative motion in the vicinity of an uncertain target – at least for the

timespan that the majority of the uncertainty distribution lies within the linear regime. Interestingly, from Eq. (5) it can be shown that some of the sensitivity terms can be influenced by control. As a result, the action of a controller has some influence on the distribution of possible relative states.

Returning to Eq. (5), the relative state sensitivity dynamics to each orbit element are derived:

$$\dot{\boldsymbol{s}}_a = \left(A_{\boldsymbol{x},a} + A_{\boldsymbol{x},\theta}\frac{\mathrm{d}\theta}{\mathrm{d}a}\right)\boldsymbol{x}^* + A_{\boldsymbol{x}}\boldsymbol{s}_a + B_{\boldsymbol{x},\theta}\frac{\mathrm{d}\theta}{\mathrm{d}a}\boldsymbol{u} \tag{11a}$$

$$\dot{\boldsymbol{s}}_{\theta_0} = A_{\boldsymbol{x},\theta}\frac{\mathrm{d}\theta}{\mathrm{d}\theta_0}\boldsymbol{x}^* + A_{\boldsymbol{x}}\boldsymbol{s}_{\theta_0} + B_{\boldsymbol{x},\theta}\frac{\mathrm{d}\theta}{\mathrm{d}\theta_0}\boldsymbol{u} \tag{11b}$$

$$\dot{\boldsymbol{s}}_i = A_{\boldsymbol{x}}\boldsymbol{s}_i + B_{\boldsymbol{x},i}\boldsymbol{u} \tag{11c}$$

$$\dot{\boldsymbol{s}}_{q_1} = \left(A_{\boldsymbol{x},q_1} + A_{\boldsymbol{x},\theta}\frac{\mathrm{d}\theta}{\mathrm{d}q_1}\right)\boldsymbol{x}^* + A_{\boldsymbol{x}}\boldsymbol{s}_{q_1} + B_{\boldsymbol{x},\theta}\frac{\mathrm{d}\theta}{\mathrm{d}q_1}\boldsymbol{u} \tag{11d}$$

$$\dot{\boldsymbol{s}}_{q_2} = \left(A_{\boldsymbol{x},q_2} + A_{\boldsymbol{x},\theta}\frac{\mathrm{d}\theta}{\mathrm{d}q_2}\right)\boldsymbol{x}^* + A_{\boldsymbol{x}}\boldsymbol{s}_{q_2} + B_{\boldsymbol{x},\theta}\frac{\mathrm{d}\theta}{\mathrm{d}q_2}\boldsymbol{u} \tag{11e}$$

$$\dot{\boldsymbol{s}}_\Omega = A_{\boldsymbol{x}}\boldsymbol{s}_\Omega + B_{\boldsymbol{x},\Omega}\boldsymbol{u} \tag{11f}$$

The unintuitive $\mathrm{d}\theta/\mathrm{d}\text{œ}_i$ terms appear due to the influence of changes in the orbit elements a, θ_0, q_1, and q_2 on the subsequent evolution of $\theta(t)$.

All terms appearing in Eq. (11) are directly computed and provided below:

$$A_{\boldsymbol{x},\text{œ}_i} = \frac{\mathrm{d}}{\mathrm{d}\,\text{œ}_i}\left(A_{\boldsymbol{x}}\right) = \begin{bmatrix} 0_{3\times3} & 0_{3\times3} \\ K_{\text{œ}_i}^{A_{\boldsymbol{x}}} & \Omega_{\text{œ}_i}^{A_{\boldsymbol{x}}} \end{bmatrix} \tag{12}$$

$$K_a^{A_{\boldsymbol{x}}} = \begin{bmatrix} -\frac{3}{a}\dot{\theta}^2 - \frac{6}{a}\frac{\mu}{r^3} & -\frac{3}{a}\ddot{\theta} & 0 \\ \frac{3}{a}\ddot{\theta} & -\frac{3}{a}\dot{\theta}^2 + \frac{3}{a}\frac{\mu}{r^3} & 0 \\ 0 & 0 & \frac{3}{a}\frac{\mu}{r^3} \end{bmatrix} \tag{13a}$$

$$\Omega_a^{A_{\boldsymbol{x}}} = \begin{bmatrix} 0 & -\frac{3}{a}\dot{\theta} & 0 \\ \frac{3}{a}\dot{\theta} & 0 & 0 \\ 0 & 0 & 0 \end{bmatrix} \tag{13b}$$

$$K_\theta^{A_{\boldsymbol{x}}} = \begin{bmatrix} 4\dot{\theta}^2\frac{\kappa'}{\kappa} + 6\frac{\mu}{r^3}\frac{\kappa'}{\kappa} & \frac{2\dot{\theta}^2}{\kappa^2}\left(4\kappa'^2 - \kappa + \eta^2\right) & 0 \\ -\frac{2\dot{\theta}^2}{\kappa^2}\left(4\kappa'^2 - \kappa + \eta^2\right) & 4\dot{\theta}^2\frac{\kappa'}{\kappa} - 3\frac{\mu}{r^3}\frac{\kappa'}{\kappa} & 0 \\ 0 & 0 & -3\frac{\mu}{r^3}\frac{\kappa'}{\kappa} \end{bmatrix} \tag{14a}$$

$$\Omega_\theta^{A_{\boldsymbol{x}}} = \begin{bmatrix} 0 & 4\dot{\theta}\frac{\kappa'}{\kappa} & 0 \\ -4\dot{\theta}\frac{\kappa'}{\kappa} & 0 & 0 \\ 0 & 0 & 0 \end{bmatrix} \tag{14b}$$

$$K_{q_1}^{A_{\boldsymbol{x}}} = \begin{bmatrix} 2\dot{\theta}^2\beta_1 + 6\frac{\mu}{r^4}\gamma_1 & 4\dot{\theta}^2\beta_1\frac{\kappa'}{\kappa} - 2\dot{\theta}^2\frac{q_2+\sin\theta}{\kappa^2} & 0 \\ -4\dot{\theta}^2\beta_1\frac{\kappa'}{\kappa} + 2\dot{\theta}^2\frac{q_2+\sin\theta}{\kappa^2} & 2\dot{\theta}^2\beta_1 - 3\frac{\mu}{r^4}\gamma_1 & 0 \\ 0 & 0 & -3\frac{\mu}{r^4}\gamma_1 \end{bmatrix} \tag{15a}$$

$$\Omega_{q_1}^{A_{\boldsymbol{x}}} = \begin{bmatrix} 0 & \frac{6}{\eta^2}q_1\dot{\theta} + \frac{4}{\kappa}\dot{\theta}\cos\theta & 0 \\ -\frac{6}{\eta^2}q_1\dot{\theta} - \frac{4}{\kappa}\dot{\theta}\cos\theta & 0 & 0 \\ 0 & 0 & 0 \end{bmatrix} \tag{15b}$$

$$K_{q_2}^{A_{\boldsymbol{x}}} = \begin{bmatrix} 2\dot{\theta}^2\beta_2 + 6\frac{\mu}{r^4}\gamma_2 & 4\dot{\theta}^2\beta_2\frac{\kappa'}{\kappa} + 2\dot{\theta}^2\frac{q_1+\cos\theta}{\kappa^2} & 0 \\ -4\dot{\theta}^2\beta_2\frac{\kappa'}{\kappa} - 2\dot{\theta}^2\frac{q_1+\cos\theta}{\kappa^2} & 2\dot{\theta}^2\beta_2 - 3\frac{\mu}{r^4}\gamma_2 & 0 \\ 0 & 0 & -3\frac{\mu}{r^4}\gamma_2 \end{bmatrix} \tag{16a}$$

$$\Omega_{q_2}^{A_{\boldsymbol{x}}} = \begin{bmatrix} 0 & \frac{6}{\eta^2}q_2\dot{\theta} + \frac{4}{\kappa}\dot{\theta}\sin\theta & 0 \\ -\frac{6}{\eta^2}q_2\dot{\theta} - \frac{4}{\kappa}\dot{\theta}\sin\theta & 0 & 0 \\ 0 & 0 & 0 \end{bmatrix} \tag{16b}$$

$$\frac{\mathrm{d}\theta}{\mathrm{d}a} = -\frac{3a\eta}{2r_0^2}\frac{\kappa^2}{\kappa_0^2}n(t-t_0) \tag{17a}$$

$$\frac{\mathrm{d}\theta}{\mathrm{d}\theta_0} = \frac{\kappa^2}{\kappa_0^2} \tag{17b}$$

$$\begin{aligned}\frac{\mathrm{d}\theta}{\mathrm{d}q_1} = \frac{1}{r^2\eta^2}\big(&r\sin\theta(r + a(1-q_1^2)) - r_0\sin\theta_0(r_0 + a(1-q_1^2)) \\ &+ aq_1q_2(r\cos\theta - r_0\cos\theta_0) + q_2(r-r_0)(a+r+r_0)\big)\end{aligned} \tag{17c}$$

$$\begin{aligned}\frac{\mathrm{d}\theta}{\mathrm{d}q_2} = \frac{1}{r^2\eta^2}\big(&-r\cos\theta(r + a(1-q_2^2)) + r_0\cos\theta_0(r_0 + a(1-q_2^2)) \\ &- aq_1q_2(r\sin\theta - r_0\sin\theta_0) - q_1(r-r_0)(a+r+r_0)\big)\end{aligned} \tag{17d}$$

$$\kappa = 1 + q_1\cos\theta + q_2\sin\theta \tag{18}$$

$$\kappa_0 = 1 + q_1\cos\theta_0 + q_2\sin\theta_0 \tag{19}$$

$$\kappa' = -q_1\sin\theta + q_2\cos\theta \tag{20}$$

$$\eta = \sqrt{1 - q_1^2 - q_2^2} \tag{21}$$

$$\beta_1 = \frac{3q_1}{\eta^2} + 2\frac{\cos\theta}{\kappa} \tag{22}$$

$$\beta_2 = \frac{3q_2}{\eta^2} + 2\frac{\sin\theta}{\kappa} \tag{23}$$

$$\gamma_1 = \frac{2aq_1}{\kappa} + \frac{a\eta^2}{\kappa^2}\cos\theta \tag{24}$$

$$\gamma_2 = \frac{2aq_2}{\kappa} + \frac{a\eta^2}{\kappa^2}\sin\theta \tag{25}$$

$$B_{\boldsymbol{x},\Omega} = \frac{\mathrm{d}B_{\boldsymbol{x}}}{\mathrm{d}\Omega} = \begin{bmatrix} 0_{3\times3} \\ -R_3(\theta)R_1(i)\tilde{\hat{\boldsymbol{e}}}_3R_3(\Omega)R_{\mathcal{NH}}^* \end{bmatrix} \tag{26a}$$

$$B_{\boldsymbol{x},i} = \frac{\mathrm{d}B_{\boldsymbol{x}}}{\mathrm{d}i} = \begin{bmatrix} 0_{3\times3} \\ -R_3(\theta)\tilde{\hat{\boldsymbol{e}}}_1R_1(i)R_3(\Omega)R_{\mathcal{NH}}^* \end{bmatrix} \tag{26b}$$

$$B_{\boldsymbol{x},\theta} = \frac{\mathrm{d}B_{\boldsymbol{x}}}{\mathrm{d}\theta} = \begin{bmatrix} 0_{3\times3} \\ -\tilde{\hat{\boldsymbol{e}}}_3R_3(\theta)R_1(i)R_3(\Omega)R_{\mathcal{NH}}^* \end{bmatrix} \tag{26c}$$

where $\tilde{\hat{\boldsymbol{e}}}_i$ denotes the skew-symmetric tilde (cross) matrix for the i^{th} basis vector.[9] Eqs. (12) - (26) are all evaluated on the nominal target orbit, and enable the sensitivity dynamics given in Eq. (5) to be computed.

Substituting $R^*_{\mathcal{NH}} = R_3^\top(\Omega^*)R_1^\top(i^*)R_3^\top(\theta^*)$, the directions for the control components u_1, u_2, u_3 track the nominal LVLH frame basis vectors. Then, Eq. (26) can be simplified when evaluated on the nominal target orbit:

$$B_{\boldsymbol{x},\Omega} = \begin{bmatrix} 0_{3\times 3} \\ -R_3(\theta)R_1(i)\tilde{\hat{\boldsymbol{e}}}_3 R_1(i)^\top R_3(\theta)^\top \end{bmatrix} = \begin{bmatrix} 0 & 0 & 0 \\ 0 & 0 & 0 \\ 0 & 0 & 0 \\ 0 & \mathrm{c}i & -\mathrm{c}\theta\mathrm{s}i \\ -\mathrm{c}i & 0 & \mathrm{s}i\mathrm{s}\theta \\ \mathrm{c}\theta\mathrm{s}i & -\mathrm{s}i\mathrm{s}\theta & 0 \end{bmatrix} \tag{27a}$$

$$B_{\boldsymbol{x},i} = \begin{bmatrix} 0_{3\times 3} \\ -R_3(\theta)\tilde{\hat{\boldsymbol{e}}}_1 R_3(\theta)^\top \end{bmatrix} = \begin{bmatrix} 0 & 0 & 0 \\ 0 & 0 & 0 \\ 0 & 0 & 0 \\ 0 & 0 & \mathrm{s}\theta \\ 0 & 0 & \mathrm{c}\theta \\ -\mathrm{s}\theta & -\mathrm{c}\theta & 0 \end{bmatrix} \tag{27b}$$

$$B_{\boldsymbol{x},\theta} = \begin{bmatrix} 0_{3\times 3} \\ -\tilde{\hat{\boldsymbol{e}}}_3 \end{bmatrix} = \begin{bmatrix} 0 & 0 & 0 \\ 0 & 0 & 0 \\ 0 & 0 & 0 \\ 0 & -1 & 0 \\ 1 & 0 & 0 \\ 0 & 0 & 0 \end{bmatrix} \tag{27c}$$

Propagating both the nominal relative state $\boldsymbol{x}^*$ and the sensitivities via Eq. (11) once, uncertainty distributions in the target orbit elements can be rapidly mapped to an evolving distribution in the relative state. This mapping is extremely accurate for close-proximity (km-scale) satellite relative motion and for modest uncertainties in the target orbit.

THE CLOHESSY-WILTSHIRE CASE

The sensitivity dynamics discussed in Section 2 for the general Keplerian relative motion problem are inconvenient to explore analytically due to their complexity. To avoid such a prolonged investigation, this section explores the sensitivity dynamics for the controlled relative motion problem when the target orbit is sufficiently near-circular to use the Clohessy-Wiltshire (CW) model.[2] It is easier to analyze this system and then afterwards investigate if and how fundamental conclusions change for the general-eccentricity case.

For the CW problem, the natural relative motion dynamics assume the following highly simplified

linear-time varying form that is a function of the target semimajor axis alone:

$$\dot{\boldsymbol{x}} = \begin{bmatrix} 0 & 0 & 0 & 1 & 0 & 0 \\ 0 & 0 & 0 & 0 & 1 & 0 \\ 0 & 0 & 0 & 0 & 0 & 1 \\ 3n^2 & 0 & 0 & 0 & 2n & 0 \\ 0 & 0 & 0 & -2n & 0 & 0 \\ 0 & 0 & -n^2 & 0 & 0 & 0 \end{bmatrix} \boldsymbol{x} \tag{28}$$

where $n = \sqrt{\mu/a^3}$. Because the CW problem linearizes about a circular orbit, the orbit element definition from Section 2 is modified. In particular, the target orbit is parameterized by a, $\overline{\theta}$, i, and Ω. The quantity $\overline{\theta}$ is measured from the ascending node, and eccentricity is assumed sufficiently small that one may write $\overline{\theta} \approx \overline{\theta}_0 + nt$. The orbit element differences are $\delta\mathbf{oe} = (\delta a, \delta\theta, \delta e, \delta i, \delta\Omega)^\top$. For this study, the chaser periapsis is located at the chaser's ascending node. Note that it is always possible to define the inertial frame such that the periapsis is at zero latitude, so there is no loss of generality with this approach.

The initial sensitivities are computed in the same manner as before – using Eq. (8). However, the mapping from element differences to local coordinates needs to be modified from Eq. (9):

$$G_{\text{CW}} = \begin{bmatrix} 1 & 0 & -a\cos\overline{\theta} & 0 & 0 \\ 0 & a & 0 & 0 & a\cos i \\ 0 & 0 & 0 & a\sin\overline{\theta} & -a\cos\overline{\theta}\sin i \\ 0 & 0 & na\sin\overline{\theta} & 0 & 0 \\ -\frac{3}{2}n & 0 & 2na\cos\overline{\theta} & 0 & 0 \\ 0 & 0 & 0 & na\cos\overline{\theta} & na\sin\overline{\theta}\sin i \end{bmatrix} \tag{29}$$

The derivatives of Eq. (29) with respect to the target orbit elements are simple and thus are not explicitly provided.

From Eqs. (8) and (28), only the sensitivity to the target semimajor axis is influenced by the relative state. Its dynamics are given with the other sensitivities below:

$$\dot{\boldsymbol{s}}_a = A_{\text{CW},a}\boldsymbol{x}^* + A_{\text{CW}}\boldsymbol{s}_a + B_{\boldsymbol{x},\theta}\frac{\mathrm{d}\overline{\theta}}{\mathrm{d}a}\boldsymbol{u} \tag{30a}$$

$$\dot{\boldsymbol{s}}_{\overline{\theta}_0} = A_{\text{CW}}\boldsymbol{s}_{\overline{\theta}_0} + B_{\boldsymbol{x},\theta}\boldsymbol{u} \tag{30b}$$

$$\dot{\boldsymbol{s}}_i = A_{\text{CW}}\boldsymbol{s}_i + B_{\boldsymbol{x},i}\boldsymbol{u} \tag{30c}$$

$$\dot{\boldsymbol{s}}_\Omega = A_{\text{CW}}\boldsymbol{s}_\Omega + B_{\boldsymbol{x},\Omega}\boldsymbol{u} \tag{30d}$$

$$A_{\text{CW},a} = \begin{bmatrix} 0 & 0 & 0 & 0 & 0 & 0 \\ 0 & 0 & 0 & 0 & 0 & 0 \\ 0 & 0 & 0 & 0 & 0 & 0 \\ -\frac{9}{a}n^2 & 0 & 0 & 0 & -\frac{3}{a}n & 0 \\ 0 & 0 & 0 & \frac{3}{a}n & 0 & 0 \\ 0 & 0 & \frac{3}{a}n^2 & 0 & 0 & 0 \end{bmatrix} \tag{31}$$

$$\frac{\mathrm{d}\overline{\theta}}{\mathrm{d}a} = -\frac{3}{2a}nt \tag{32}$$

Inspecting Eqs. (30) – (32), the influence of control and the motion of the nominal trajectory are generally sub-dominant in the dynamics of $\boldsymbol{s}_a$. In other words, $\dot{\boldsymbol{s}}_a \approx A_{\text{CW}}\boldsymbol{s}_a$, except for large magnitudes of the control signal $\boldsymbol{u}$, or large values of the components of the nominal relative state $\boldsymbol{x}^*$.

Further interpretation of the sensitivity dynamics for the CW case is possible by investigating the initial values of the sensitivities themselves using Eq. (8). Note that the uncontrolled dynamics of $\boldsymbol{s}_{\theta_0}$, $\boldsymbol{s}_i$, and $\boldsymbol{s}_\Omega$ are all the same as the CW system. It can be shown that all three are periodic. Consider $\boldsymbol{s}_{\theta_0}(0)$:

$$\boldsymbol{s}_{\theta_0}(0) = \begin{pmatrix} a\sin\overline{\theta}_0\delta e \\ -a \\ a\cos\overline{\theta}_0\delta i + a\sin\overline{\theta}_0\sin i\delta\Omega \\ na\cos\overline{\theta}_0\delta e \\ -2na\sin\overline{\theta}_0\delta e \\ -na\sin\overline{\theta}_0\delta i + na\cos\overline{\theta}_0\sin i\delta\Omega \end{pmatrix} \tag{33}$$

The CW no-drift condition is $\dot{y}_0 + 2nx_0 = 0$. From Eq. (33), the components $s_{\theta_0,x}(0)$ and $s_{\theta_0,\dot{y}}(0)$ satisfy this constraint. Additionally, $s_{\theta_0,y}$ is much greater than all other components of $\boldsymbol{s}_{\theta_0}$ and is nearly stationary in the absence of control. it A similar result can be shown for $\boldsymbol{s}_i$ and $\boldsymbol{s}_\Omega$ using their initial components – both of these sensitivities are also periodic in the uncontrolled case. For $\boldsymbol{s}_i$, the dominant component is a large periodic oscillation in $s_{i,z}$, with the state components in the x and y directions of a negligible scale by comparison. For $\boldsymbol{s}_\Omega$, there is a large y component, and the oscillatory z component is also large, whereas the x component is insignificant.

Because the sensitivities directly map static uncertainty distributions in $\boldsymbol{\alpha}\mathbf{e}_0$ to evolving uncertainty distributions in the relative state, it is of interest to see which sensitivities drive the growth in the distribution in the absence of control. Because all other sensitivities are periodic, is clear that growth in components of $\boldsymbol{s}_a$ must be driving the secular growth in uncertainty for uncontrolled relative motion. The unforced behavior of $\boldsymbol{s}_a$ turns out to be extremely simple. To start out, the initial value of the sensitivity is given below:

$$\boldsymbol{s}_a(0) = \begin{pmatrix} -1 - \cos\overline{\theta}_0\delta e \\ \delta\overline{\theta}_0 + \cos i\delta\Omega \\ \sin\overline{\theta}_0\delta i - \cos\overline{\theta}_0\sin i\delta\Omega \\ -\frac{1}{2}n\sin\overline{\theta}_0\delta e \\ \frac{3}{2}n + \frac{9n}{4a}\delta a - n\cos\overline{\theta}_0\delta e \\ -\frac{n}{2}\cos\overline{\theta}_0\delta i - \frac{n}{2}\sin\overline{\theta}_0\sin i\delta\Omega \end{pmatrix} \tag{34}$$

Substituting the initial sensitivity state into the CW solution[9] and keeping only dominant terms, the sensitivity to semimajor displays the following approximate behavior, neglecting small oscillations:

$$\boldsymbol{s}_a(t) \approx \left(-1,\ \frac{3}{2}nt,\ 0,\ 0,\ \frac{3}{2}n,\ 0\right)^\top \tag{35}$$

It is natural to ask what the influence of control on the sensitivities can have – because any permitted purposeful control of the sensitivities enables a corresponding control of some aspect of the evolving relative state uncertainty distribution. To answer this, first recall that the scale of control needed to significantly influence $\boldsymbol{s}_a$ is of a much larger scale than that needed for the

other sensitivities, due to the n/a multiplier on the control $\boldsymbol{u}$. Thus, the controllability of the other sensitivities $\boldsymbol{s}_{\theta_0}$, $\boldsymbol{s}_i$, and $\boldsymbol{s}_\Omega$ with lower thrust is considered. For control analyses of this type, the resulting meager effect of control on $\boldsymbol{s}_a$ is neglected. Furthermore, the z components of the sensitivities are decoupled from the in-plane components and are also neutrally stable, so these will be ignored as well.

Note that it can be determined from Eqs. (30) and (27) that the simultaneous control of all components of $\boldsymbol{x}^*$, $\boldsymbol{s}_{\theta_0}$, $\boldsymbol{s}_i$, and $\boldsymbol{s}_\Omega$ is impossible. However, control of a subset of these states is possible. As a demonstration of control of a subset of the sensitivities, a simple strategy is explored in this paper that combines augmented control of the planar $\boldsymbol{x}^*$ and $\boldsymbol{s}_{\theta_0}$ with stabilization of planar $\boldsymbol{s}_\Omega$. The out-of-plane components of the nominal relative state and the sensitivities are ignored. The augmented dynamics are given below:

$$\dot{\boldsymbol{z}} = \frac{\mathrm{d}}{\mathrm{d}t}\begin{pmatrix} \boldsymbol{x}_{\mathrm{2D}} \\ \boldsymbol{s}_{\theta_0,\mathrm{2D}} \end{pmatrix} = \begin{bmatrix} A_{\mathrm{2D}} & 0_{4\times4} \\ 0_{4\times4} & A_{\mathrm{2D}} \end{bmatrix} \boldsymbol{z} + B_{\boldsymbol{z}}\boldsymbol{u} \tag{36}$$

where the control vector is composed of the in-plane accelerations $\boldsymbol{u} = (a_x,\ a_y)^\top$, and A_{2D} and $B_{\boldsymbol{z}}$ are given below:

$$A_{\mathrm{2D}} = \begin{bmatrix} 0 & 0 & 1 & 0 \\ 0 & 0 & 0 & 1 \\ 3n^2 & 0 & 0 & 2n \\ 0 & 0 & -2n & 0 \end{bmatrix} \tag{37}$$

$$B_{\boldsymbol{z}} = \begin{bmatrix} 0 & 0 & 1 & 0 & 0 & 0 & 0 & 1 \\ 0 & 0 & 0 & 1 & 0 & 0 & -1 & 0 \end{bmatrix}^\top \tag{38}$$

Stabilization of $\boldsymbol{s}_\Omega$ is achieved by enforcing the no-drift constraint $x_{\mathrm{off}}(\boldsymbol{s}_\Omega) = 4s_{\Omega,x} + \frac{2}{n}s_{\Omega,\dot{y}} \approx 0$ to prevent secular growth in the $\boldsymbol{s}_\Omega$ dynamics. This is achieved by the following out-of-plane control component:

$$u_3 = a_z = \frac{\cos i}{\sin i \sin\overline{\theta}} u_1 \tag{39}$$

where some maximum $|u_3| < \delta$ is enforced as needed for when $\sin\overline{\theta}$ is small. Computing the controllability matrix $\mathcal{C} = [B\ AB\ A^2B \ldots A^7B]$ for the LTI system given by Eq. (36), the rank is 8, thus the augmented planar state and θ_0 sensitivity dynamics are determined to be fully controllable. Most of the secondary effects of the control strategy are small changes in the neutrally stable out-of-plane components of the sensitivities $\boldsymbol{s}_i$ and $\boldsymbol{s}_\Omega$, and increases in the out-of-plane motion of $\boldsymbol{x}^*$. Additionally, this strategy does have a tendency to grow the small in-plane components of $\boldsymbol{s}_i$. Nonetheless, it is a simple demonstration of the possibility of designing control to influence the sensitivities.

NUMERICAL SIMULATIONS

Efficient Relative State Uncertainty Propagation via the Sensitivities

To demonstrate the successful propagation of the sensitivity dynamics for the general Keplerian case, consider the example given by the information in Table 1. For this example, the initial target orbit element error statistics correspond to uncertainty in its initial orbit position on the order of 100 m, with cm/s error in velocity. The chaser spacecraft orbit position is assumed perfectly known, but the relative state is uncertain. The nominal relative state is linearly propagated using the plant

matrix given by Eq. (6) and the sensitivities are propagated from their initial values – obtained using Eq. (8) – through use of Eq. (11) . This first study is control-free, investigating the behavior of the unforced sensitivities over the course of two nominal target orbit periods. The dominant

Table 1: Eccentric Target Orbit, Unforced Relative Motion

Parameters	Values
Nominal Target Orbit	$\mathbf{oe}^*_{t,0} = (a, e, i, \omega, \Omega, f_0) \approx (12600 \text{ km},\ 0.3,\ 63.4^\circ,\ 27^\circ,\ 2^\circ,\ 10^\circ)$ $\theta^*_0 = 37^\circ,\ q^*_1 = 0.2673,\ q^*_2 = 0.1362$
Target Orbit Uncertainty	Normal dist., zero-mean, angle deviations $\times 10^{-5}$ degrees: $\sigma_a = 20$ m, $\sigma_e = 2 \times 10^{-6}, \sigma_i = 4, \sigma_\omega = 4,\ \sigma_\Omega = 1.9,\ \sigma_{f_0} = 8$
Chaser Spacecraft Orbit	$\delta\mathbf{oe}^*_{s,0} = \mathbf{oe}_{s,0} - \mathbf{oe}^*_{t,0} = (0.4 \text{ km},\ 8 \times 10^{-5},\ 0.01^\circ,\ 0.006^\circ,\ 0^\circ,\ 0^\circ)$
Nominal Initial Relative State	$\boldsymbol{\rho}_0 = (-724.2,\ 926.9,\ 929.7)$ m, $\boldsymbol{\rho}'_0 = (0.009,\ 1.202,\ 1.097)$ m/s

components of the sensitivities of relative position to each orbit element are given in Figures. 2 - 5. The sensitivities of velocity are not explicitly shown but their behavior can be inferred from the position sensitivity curves, because the sensitivities behave like augmented position and velocity state vectors. Inspecting the sensitivity figures, the out-of-plane components of sensitivities to semimajor axis and θ_0 are negligible, and so are the in-plane components of sensitivity to inclination. Note that all sensitivities except $\boldsymbol{s}_a$ are periodic, thus it is the uncertainty in target semimajor axis that drives secular growth in relative state uncertainty. This finding agrees with intuition, because only an error in the target semimajor axis would correspond to a drift over time.

The effect of the scale of target eccentricity on the sensitivities is straightforward. For low eccentricity, the growth in $s_{a,y}$ becomes more linear in time, and the oscillations in $s_{a,x}$ are reduced. As $e \to 0$, $s_{a,x} \to -1$. Additionally, for low eccentricity, the $s_{\theta_0,x}$ curve is composed of small oscillations about zero, and the $s_{\theta_0,y}$ curve is nearly constant, oscillating about $-a^*$. For larger values of eccentricity, the oscillations in $\boldsymbol{s}_{\theta_0}$ become large, as demonstrated by the large oscillations in the two quantities for $e = 0.3$ in Figure 3. The characteristic behavior of $\boldsymbol{s}_i$, $\boldsymbol{s}_{q_1}$, and $\boldsymbol{s}_{q_2}$ does not change greatly with the eccentricity except for an increasing sharpness near target periapsis for very high values of eccentricity. For $\boldsymbol{s}_\Omega$, the oscillations in the y component flatten out as eccentricity is decreased.

Note that the scale of components of $\boldsymbol{s}_a$ is smaller than the components of sensitivities to the target orbit element angles because small variations in angular separation scale with the semimajor axis of the orbit, so even a small error in θ_0 can have large consequences for the relative state in Cartesian components. Rescaling $\underline{s}_a = a^* \boldsymbol{s}_a$ might be a superior way of representing the scale of the sensitivities to semimajor axis – mapping small deviations in $(a - a^*)/a^*$ to large variations in the x and y coordinates of the relative state.

The real value of propagating the sensitivities is in their use for rapidly and accurately capturing variations in the relative state arising from uncertainty in the target orbit. The sensitivities are propagated once by evaluating their linear equations on a nominal target orbit, and the nominal relative state is also propagated once using the nominal target orbit. Then, dispersions in the target orbit elements from its nominal values can be directly mapped to dispersions in the local relative state using Eq. (10). To demonstrate the usefulness of this, the statistical variations in the initial target orbit elements given in Table 1 are used to generate a 1000-point Monte Carlo study of the evolution of the relative state. To investigate collision risk, the time of smallest relative distance for

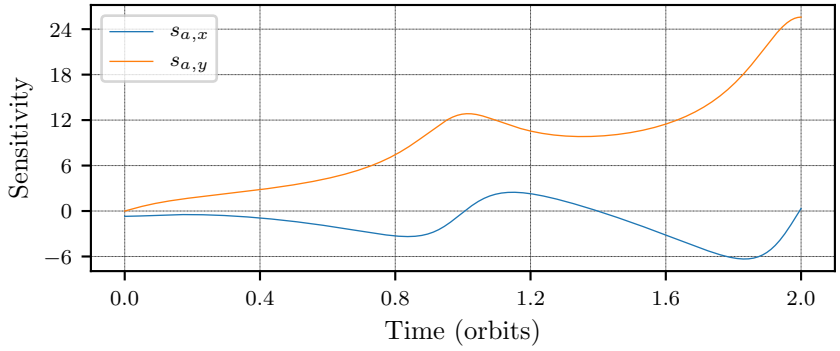

Figure 2: Relative Position Sensitivities to Target Semimajor Axis

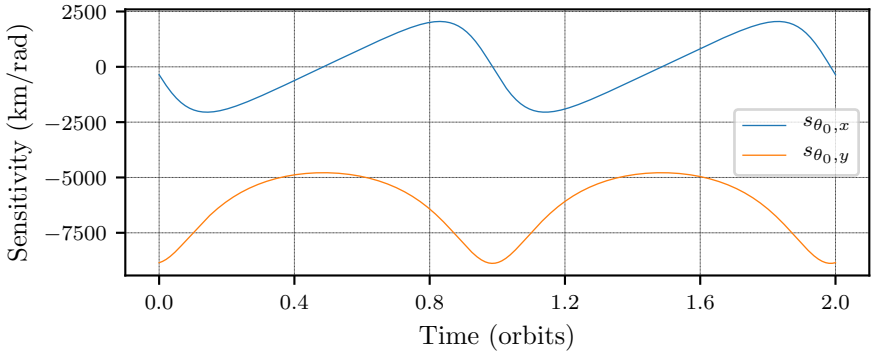

Figure 3: Relative Position Sensitivities to Target Initial Argument of Latitude

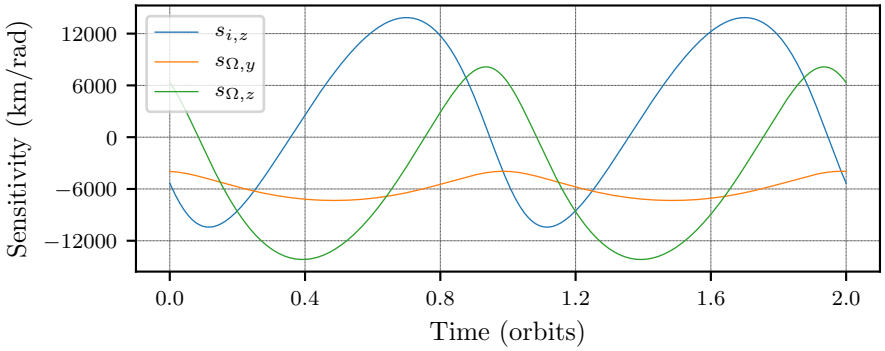

Figure 4: Relative Position Sensitivities to Target R.A.A.N and Inclination

the nominal relative trajectory is computed to be $t_{\text{crit}} \approx t_0 + 1.328T^*$. All 1000 points are given in Figure 6 at times t_0 (blue) and t_{crit} (red), along with a subset of their connecting trajectories (gray) and the nominal trajectory (dashed line). This information is all obtained in a matter of seconds, because the individual points do not need to be numerically propagated and are instead mapped directly through the sensitivities. Repeating this study with 10,000 points thus results in minimal increase in runtime. Comparing the sensitivity-mapped relative state solutions to their true values obtained by numerical integration of the individual cases, the sensitivity study is revealed to be highly accurate, with none of the position errors ever exceeding 0.2 cm in the simulated timespan

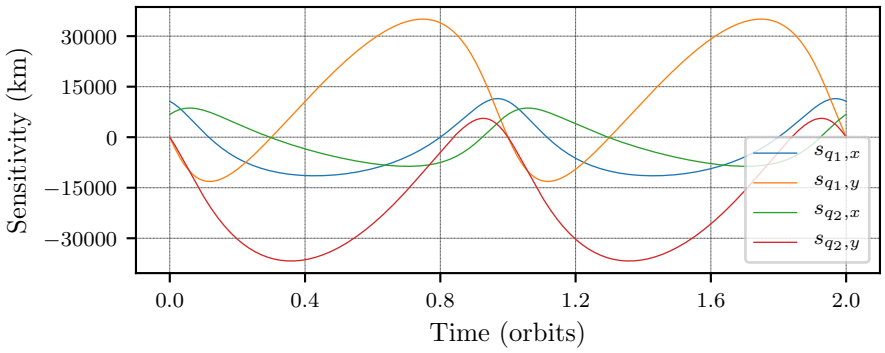

Figure 5: Relative Position Sensitivities to Target q_1, q_2

of 1.328 nominal target orbit periods.

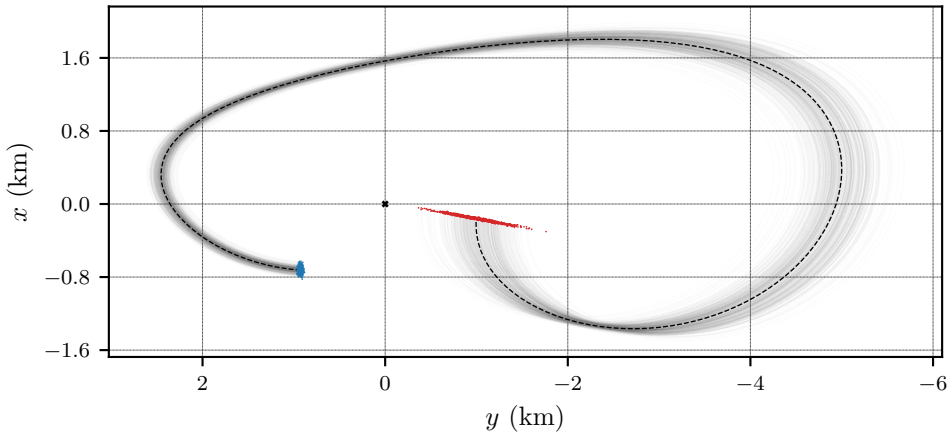

Figure 6: Sensitivity-Propagated Relative State Uncertainty Distribution

The relative states depicted in Figure 6 are each results for different target orbits – the relative motion is shown in the nominal LVLH frame centered on the uncertain target at $(0,\ 0)$. The chaser spacecraft orbit is known, but the target-centered relative state is unknown due to target orbit uncertainty. As expected, this relative state uncertainty grows over time, discernible from the spread in the initial relative positions (blue) to the spread in final relative positions (red) in Figure 6. This is an interesting result because a single linear simulation allows very large samples of possible relative states to be propagated efficiently, despite the fact that each of these points is for a different target orbit and would traditionally require its own linearization.

Overall, this method tends to work quite well for at least one target orbit period for uncertainties in the target orbit corresponding to up to km-scale initial position error in low Earth orbits. The sensitivities enable efficient characterization of the evolving uncertain relative state for proximity operations in the vicinity of an uncertain target object. Additionally, they enable a direct study of which target orbit element uncertainties are the largest contributors to the relative state error at a future time of interest. Because it relies on linearized dynamics of the relative state's sensitivity to target orbit elements, it breaks down with both large separations in the nominal relative state and with sufficiently large differences between the nominal target orbit and the true orbit. As a result,

the accuracy of the method will degrade for target orbit statistics with large standard deviations in the initial orbit elements. The method is fairly sensitive to errors in semimajor axis, which must be known to a certainty of kilometers or better. Nonetheless, it is quite useful for situations with modest uncertainty in the target object orbit.

Control Examples with the CW System

To test the influence of control on the sensitivities, this paper explores simple examples of infinite-time LQR control with the CW dynamics. The following cost is minimized for symmetric positive-definite Q and R:

$$J = \int_{t_0}^{\infty} \left(\boldsymbol{x}^\top Q \boldsymbol{x} + \boldsymbol{u}^\top R \boldsymbol{u} \right) \mathrm{d}t \tag{40}$$

The cost-minimizing feedback control is $\boldsymbol{u} = -R^{-1} B^\top P \boldsymbol{x}$ where P solves the algebraic Riccati equation:

$$A^\top P + PA - PBR^{-1}B^\top P + Q = 0 \tag{41}$$

Naïve Relative State Control Note that typical control maneuvers conducted in close-proximity exert only a small influence on the sensitivities. This is especially true if the control effort for the maneuvers is low. As an example, consider the case given by the data in Table 2.

Table 2: Simulation Parameters, CW Control Example 1

Parameters	Values
Nominal Target Orbit Elements	$a^* = 8000$ km, $\overline{\theta}_0^* = 37^\circ$, $i^* = 30^\circ$, $\Omega^* = 21^\circ$
Target Orbit Uncertainty	Normal dist., zero-mean, angle deviations $\times 10^{-5}$ degrees: $\sigma_a = 6.0$ m, $\sigma_i = 4.0$, $\sigma_\Omega = 1.9$, $\sigma_{\overline{\theta}_0} = 8.0$
Nominal Initial Relative State	$\boldsymbol{\rho}_0 = (-0.92, -2.92, -3.76)$ km, $\boldsymbol{\rho}_0' = (1.27,\ 2.06,\ -5.22)$ m/s
Target Relative Motion	Bounded relative orbit, $x(0) = 0.5$ km, $\dot{y}(0) = -2n^* x(0)$
Control Parameters	$Q_{\boldsymbol{\rho}\boldsymbol{\rho}} = 2I_{3\times3}$, $Q_{\boldsymbol{\rho}'\boldsymbol{\rho}'} = 100 I_{3\times3}$, $R = 10^{13} I_{3\times3}$
Simulation Parameters	$t_f = 2.25\, T^*$

The optimal control signal solving the infinite-time LQR problem parameterized by Table 2 is not very aggressive, taking about 2 nominal target orbit periods to settle 95% of the initial relative state error. The resulting nominal relative motion is given by the dotted line in Figure 7. The achieved nominal relative orbit is approximately 2 km by 1 km. To simulate the effects of uncertainty in the target orbit, a 1000-point Monte Carlo study is also propagated using the sensitivities for the CW case, whose dynamics are given by Eq. (30). None of the sensitivity-propagated controlled relative position errors exceed 5 cm from their true values in the 2.25 nominal orbit periods simulated. This demonstrates that the sensitivities remain effective for efficiently studying relative state outcomes for cases of controlled relative motion.

The most significant relative state sensitivities are given in Figures 8 and 9. Note that the sensitivities for relative state propagation without control are given as dotted black lines that are very close to their counterparts from the controlled example (colored). This shows that the control strategy explored for this example exerts only a small influence on the sensitivities. This is because the relative state sensitivities are more costly to significantly influence than the relative state. First, for the sensitivity to semimajor axis, Eqs. (30) and (32) show that the influence of control on the dynamics

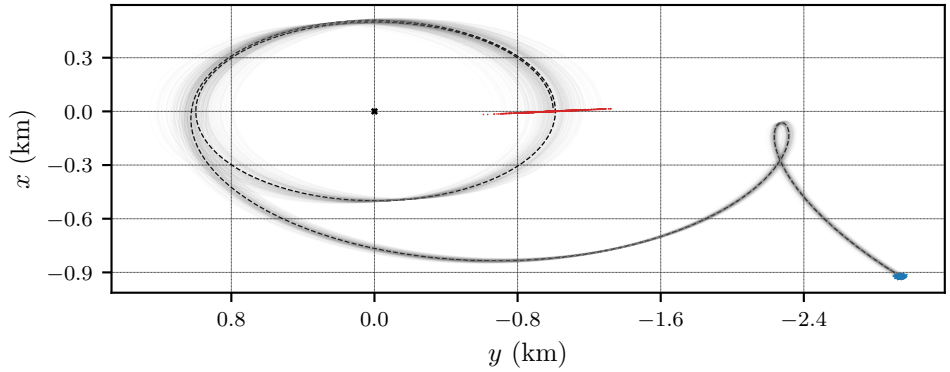

Figure 7: Controlled Relative State, Naïve Control Example

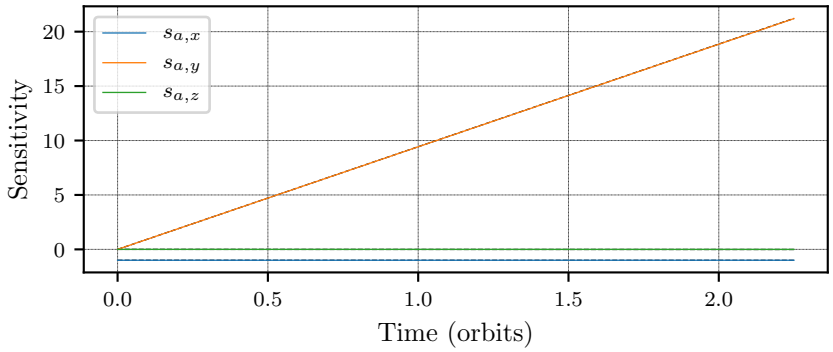

Figure 8: Sensitivity to Semimajor Axis, Naïve Control Example

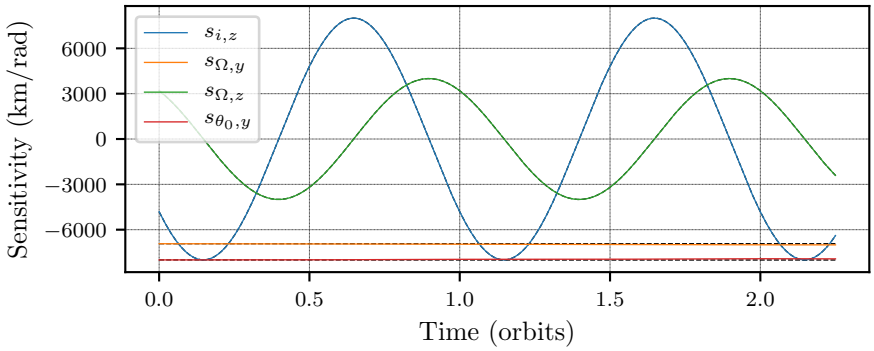

Figure 9: Sensitivities to Target Orbit Element Angles, Naïve Control Example

is pre-multiplied by n^*/a, a very small quantity. For the sensitivities to Ω, i, and $\overline{\theta}_0$, the reason for the weak influence of control is due to the sheer scale of those sensitivity states, which are much larger than the relative state. Recall from Eq. (30) that these sensitivities obey forced CW dynamics, just like the relative state. There are actually comparable effects of control on the relative state and the sensitivities - the control exerts a km-scale influence on the relative state, and a km/rad scale influence on the sensitivities. The sensitivities are simply quite costly to influence significantly, at least in comparison to the cost of achieving desired regulation and tracking control of the relative

state. This is an important point that will be discussed further in the next control example.

Note from Figures 8 and 9 that the simple predictions of Eqs. (33) - (35) and their associated discussions in Section 3 are accurate. In particular, for $\boldsymbol{s}_i$, the dominant component is a large periodic oscillation in $s_{i,z}$, with the state components in the x and y directions of a negligible scale by comparison. For $\boldsymbol{s}_\Omega$, there is a large y component, and the oscillatory z component is also large, whereas the x component is insignificant (not shown). Additionally, by inspection of Figure 8, the simple secular behavior given by Eq. (35) for $\boldsymbol{s}_a$ is also shown to be accurate.

Comparing the curves in Figures 8 and 9 with their counterparts in Figures 2 - 5 for an eccentric target orbit, the qualitative differences in the sensitivity between the circular target and eccentric target orbit cases are fairly straightforward. First, the oscillations in $s_{a,x}$ and $s_{a,y}$ become more pronounced, but the secular growth in $s_{a,y}$ is retained for both. Next, because the target orbit is now circular, the in-plane sensitivities of the relative state to target elements Ω and θ_0 no longer vary considerably over time. Lastly, because the target orbit is assumed circular and the dynamic effects of nonzero target orbit eccentricity are not at all considered by the CW formulation, the sensitivities s_{q_1} and s_{q_2} are undefined here.

Augmented Relative State and Sensitivity Control As an example of combined control of the relative state and a subset of the sensitivities, the strategy discussed in Section 3 is implemented. This strategy maneuvers the spacecraft to a desired final relative state, and in the process, reduces the planar relative state sensitivity to θ_0 while preserving the planar sensitivity to Ω. In general, this results in an exaggeration of the neutrally stable out-of-plane motion, while also potentially generating insignificant increases in the in-plane sensitivity of the relative state to the target inclination. For this example, the relevant simulation parameters are provided in Table 3.

Table 3: Simulation Parameters, CW Control Example 2

Parameters	Values
Nominal Target Orbit Elements	$a^* = 8000$ km, $\overline{\theta}_0^* = 37°$, $i^* = 30°$, $\Omega^* = 21°$
Nominal Initial Relative State	$\boldsymbol{\rho}_0 = (-0.92, -2.92, -3.76)$ km, $\boldsymbol{\rho}' = (1.27,\ 2.06,\ -5.22)$ m/s
Control Goals	$\boldsymbol{\rho}_{2\text{D}} = (0, -4)$ km, $\boldsymbol{\rho}'_{2\text{D}} = (0, 0)$ m/s,
	$s_{\overline{\theta}_0,x} = 0$ km/rad, $s_{\overline{\theta}_0,y} = -7200$ km/rad (10% reduction)
	Preserve $\boldsymbol{s}_\Omega$, ignore out-of-plane relative state and sensitivities
Control Parameters	$Q = \text{diag}(200, 200, 10^4, 10^4, 0.02, 0.02, 10, 10)$, $R = 10^{11} I_{2\times 2}$,
	Out-of-plane control $u_3 = \frac{\cos i}{\sin i \sin \overline{\theta}} u_1$, $\lvert u_3 \rvert < 1$ m/s^2
Simulation Parameters	$t_f = 4.0\ T^*$

In general, it has been determined that controlling the sensitivities is more costly than control of the relative state. As a simple demonstration of the possibility of controlling the relative state along with a subset of the sensitivities, a stationary along-track offset of 4 km is targeted, in a control maneuver that also yields a 10% reduction in the magnitude of $s_{\overline{\theta}_0,y}$, while keeping $s_{\overline{\theta}_0,x} \approx 0$ and preserving the values of the planar components of $\boldsymbol{s}_\Omega$. Through this action, the contribution of uncertainty in the target orbit element $\overline{\theta}_0$ to uncertainty in the relative state is reduced. The purpose of this control example is to demonstrate that the sensitivities can be meaningfully influenced by control action.

Using the augmented control design discussed in Section 3 and the control parameters in Table 3, the control effect is simulated for 4 nominal target orbit periods. The resulting motion of the

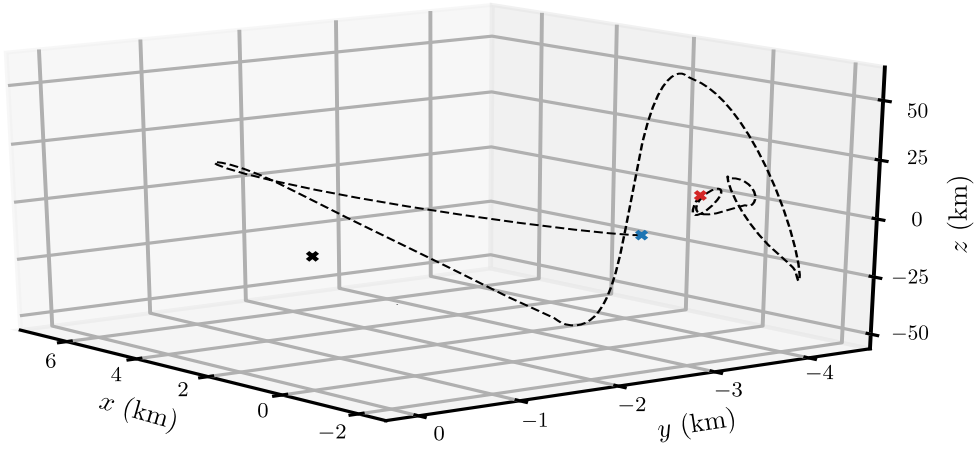

Figure 10: Relative Motion Trajectory, Augmented Control Example

nominal trajectory is given in Figure 10. The initial point is given by a blue x and the final point is given by a red x, and the target is at the origin of the nominal LVLH frame, indicated with a black x. Note from Figure 10 that the relative state trajectory follows a very indirect path to the target relative position. This is because a lot of control effort has to be exerted to reduce the planar components of $\boldsymbol{s}_{\bar{\theta}_0}$ as specified. There is no way to exert this control effort without also affecting the relative state in the process.

The time-varying behaviors of each component of the controlled nominal relative position are given in Figure 11. Examining both Figures 10 and 11, the initial large change in the relative position is clear. There is an almost 8 km shift in x and a $\sim$ 2 km shift in y. This maneuver seems necessary to initialize reduction in $s_{\bar{\theta}_0,y}$. Using other control simulations, it is determined that the size of this initial maneuver scales with the desired reduction in $s_{\bar{\theta}_0,y}$. Despite this large initial deviation, the relative state does eventually settle to the desired value, as can be seen from Figure 11. The planar relative position settles to the desired values $x = 0$, $y = -4$. These desired values are indicated by the two horizontal dashed lines.

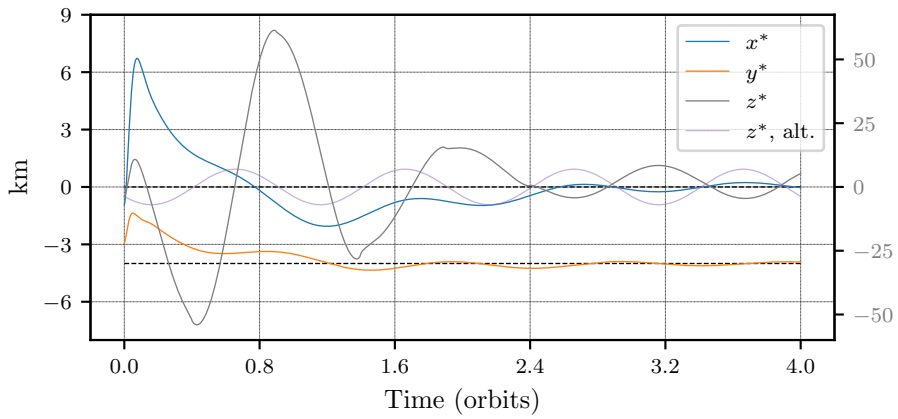

Figure 11: Relative Position, Augmented Control Example

Note that as a consequence of the control compensation given by Eq. (39), the out-of-plane

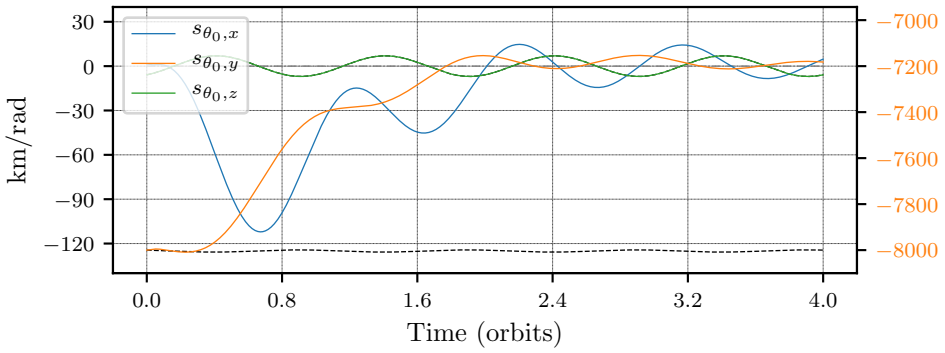

Figure 12: Controlled Sensitivity to θ_0, Augmented Control Example

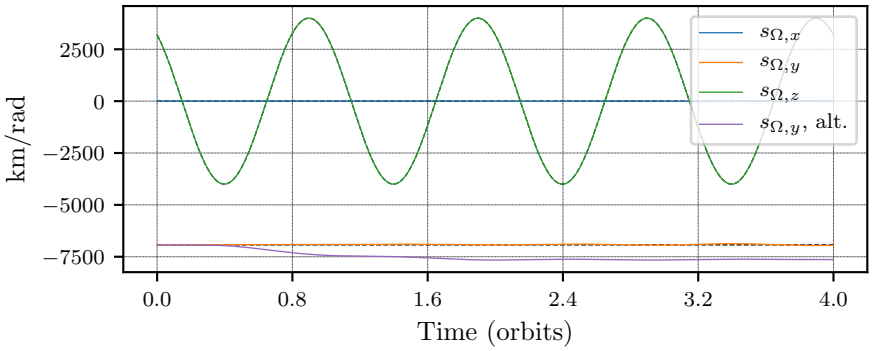

Figure 13: Stationary Sensitivity to Ω, Augmented Control Example

motion is highly affected, as indicated by the gray curve in Figure 11. The out-of-plane nominal relative state oscillations would be limited to $|z| < 2$ km without this compensation strategy (purple curve), but grow to oscillations of up to $|z| < 9$ km, especially in the first 1.5 orbits. Note that the out-of-plane motion settles to smaller variations after 2.4 orbits. However, without the control compensation strategy, there would be larger changes in $\boldsymbol{s}_\Omega$. This is clear from examining Figure 13. Without the control compensation, $u_3 = 0$, and $s_{\Omega,y}$ is heavily affected. This is given by the purple curve, while the properly stabilized behavior of $s_{\Omega,y}$ is shown by the orange curve.

The position components of $\boldsymbol{s}_{\bar{\theta}_0}$ are given in Figure 12. The 10% reduction in the absolute value of $s_{\bar{\theta}_0,y}$ is achieved. The uncontrolled $s_{\bar{\theta}_0,y}$ is given by the dashed horizontal curve towards the bottom of the plot, while the orange curve shows the effect of control on that component. Note the large scale of $s_{\bar{\theta}_0,y}$ necessitates that it be plotted with its own y axis, on the right side of the plot. This enables small details in the other two components to be discernible. The small oscillations in $s_{\bar{\theta}_0,z}$ are essentially unaffected, and the component $s_{\bar{\theta}_0,x}$ is successfully regulated.

Finally, the control components for this example are given in Figure 14. Note from Eq. (39) that $|u_3| \to \infty$ as $\sin\bar{\theta} \to 0$, but this is avoided by enforcing $|u_3| < 1$ m/s^2. Nonetheless, the control signal prescribed in Figure 14 might be a challenge to implement practically, due to the combination of small and medium accelerations needed, and especially by the challenging profile of $u_3(t)$. Additionally, a more ambitious control strategy than what is explored with this second example is probably possible. These things are beyond the scope of this work, which only introduces the sensitivity dynamics and does a preliminary investigation of whether or not they can be influenced by

control. From this second control example, it is clear that the sensitivities can be meaningfully influenced by control, but it is costly, and difficult to balance with relative state control requirements. As discussed previously, because the components of the sensitivities are so large, more control action must be exerted to significantly change these than to significantly change the relative state.

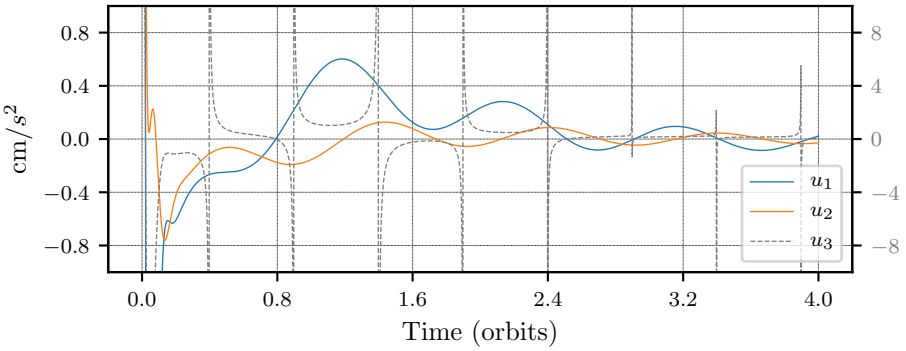

Figure 14: Control Accelerations, Augmented Control Example

This last point is an important insight of this work. It is an appealing concept to directly control some aspects of the evolving relative state uncertainty distribution, but it doesn't seem to always be practical. The most practical way to ensure safe relative motion is to design relative motion while being aware of the distribution of possible relative states for a chosen maneuver design. It is much easier to move the entire relative state distribution than it is to significantly contract it in particular directions. Inspecting Figure 7 for example, it is apparent that considering the nominal relative state alone in relative motion control design can be dangerous, because there is a risk for impact depending on how the uncertainty distribution evolves. Computing the sensitivities along with the nominal relative state response to a control action enables safe relative motion control in the presence of target orbit uncertainty to be executed very efficiently. Finally, note that there are limits to what control can achieve when influencing the relative state uncertainty distribution – changing the shape is possible, but greatly reducing the volume through the action of control alone should be impossible. Only measurements can effectively curb uncertainty growth.

CONCLUSIONS

This paper explores the sensitivities of the relative state to initial target orbit elements in the satellite relative motion problem. The initial values and the dynamics of the sensitivities are derived for the case of any target orbit eccentricity and for the special case that the target orbit is circular. Simulations performed show that the sensitivities can be used to efficiently study how the uncertain relative state distribution evolves with high accuracy. The sensitivities can be used to directly map from uncertainty distributions in the initial target orbit elements to the consequential evolving uncertainty distribution in the relative state. This enables rapid characterization of statistical risks of impact for the case of maneuvering in the vicinity of an uncertain target object. This would be especially useful in instances where the target object cannot be continuously tracked.

To explore the effects of relative state control on the sensitivities, infinite-time LQR control is implemented with the CW system. The effects of control on the sensitivities are determined to typically be fairly small, because the sensitivities to target elements tend to have much larger state values than those of the relative state, and are thus more difficult to significantly alter. The prospect

of augmented control of a subset of the sensitivities with the nominal relative state is also briefly explored in this paper, testing a formulation that controls planar relative state and planar sensitivity to the initial target of argument latitude while preserving sensitivity to target R.A.A.N. This simple control design is implemented with infinite-time LQR and achieves the desired control objectives. It is observed that inducing large changes in the sensitivities is fairly expensive, and in practice it would often be easier to simply control the relative state directly while computing the effects of such control actions on the uncertainty distribution via the sensitivities.

The concept of rendezvous and relative motion control in the vicinity of an uncertain orbit is not new. However, the formulation discussed in this paper offers new perspectives. The sensitivity dynamics are shown to be rather simple, behaving like the relative motion dynamics but forced by control and by the relative state in some cases. There are several ways this work can be expanded on in the future. First, analytic solutions of the relative state sensitivities to the target orbit elements could be derived. Combined with a suitable analytic formulation for propagating the relative state, such as by using the Tschauner-Hempel equations,[10] this would remove the need for any numerical integration when studying the problem of maneuvering in the vicinity of a poorly tracked target object. Additionally, the full problem could be explored – including sensitivities of the relative state to both the initial target and chaser orbit elements. While maneuvering space objects are typically well-tracked, the small error in the chaser spacecraft's orbital state can still be important in the uncertain relative motion problem. Additionally, more exploration of the limitations of the augmented control of the relative state and sensitivities would be useful. Lastly, the sensitivity formulation can in principle be used to design control that reduces the statistical risk of collision.

REFERENCES

[1] Louis Breger and Jonathan P. How. Safe Trajectories for Autonomous Rendezvous of Spacecraft. *Journal of Guidance, Control, and Dynamics*, 31(5):1478–1489, 2008.

[2] W. H. Clohessy and R. S. Wiltshire. Terminal Guidance System for Satellite Rendezvous. *Journal of the Aerospace Sciences*, 27(9):653–658, Sept. 1960.

[3] Dong-Woo Gim and Kyle T. Alfriend. The state transition matrix of relative motion for the perturbed non-circular reference orbit. *AIAA Journal of Guidance, Control, and Dynamics*, 26(6):956–971, 2003.

[4] M. Holzinger, J. DiMatteo, J. Schwartz, and M. Milam. Passively safe Receding Horizon Control for satellite proximity operations. In *2008 47th IEEE Conference on Decision and Control*, pages 3433–3440, Dec 2008.

[5] Stephen Kahne. Low-Sensitivity Design of Optimal Linear Control Systems. *IEEE Transactions on Aerospace and Electronic Systems*, 4(3):374–379, May 1968.

[6] Robin Larsson, Joseph Mueller, Stephanie Thomas, Björn Jakobsson, and Per Bodin. Orbit constellation safety on the PRISMA in-orbit formation flying test bed. In *Proceedings of the 3rd International Symposium on Formation Flying, Missions and Technologies, ESA-ESTEC*, number 654 SP in European Space Agency, (Special Publication) ESA SP, November 2008. 3rd International Symposium on Formation Flying, Missions and Technologies, ESA-ESTEC ; Conference date: 23-04-2008 Through 24-04-2008.

[7] Sangjin Lee, Hao Lyu, and Inseok Hwang. Analytical Uncertainty Propagation for Satellite Relative Motion Along Elliptic Orbits. *Journal of Guidance, Control, and Dynamics*, 39(7):1593–1601, 2016.

[8] Zhan Li, Xuebo Yang, and Huijun Gao. Autonomous impulsive rendezvous for spacecraft under orbital uncertainty and thruster faults. *Journal of the Franklin Institute*, 350(9):2455–2473, 2013.

[9] Hanspeter Schaub and John L. Junkins. *Analytical Mechanics of Space Systems*. AIAA Education Series, Reston, VA, 4th edition, 2018.

[10] J. Tschauner and P. Hempel. Rendezvous zu einem in elliptischer bahn umlaufenden ziel. *Astronautica Acta*, 11(5):104–109, 1965.

[11] C. Zhang, P. Melin, Shu-Nan Wu, Wen-Ya Zhou, Shu-Jun Tan, and Guo-Qiang Wu. Robust H-Infinity Control for Spacecraft Rendezvous with a Noncooperative Target. *The Scientific World Journal*, 2013:579703, 2013.